Novel porous carbons derived from coal tar rejects

Novel Porous Carbons derived from Coal Tar Rejects: Assessment of the Role of Pore Texture in CO_2 Capture under Realistic Post-combustion Operating Temperatures

Enrique García-Díez[†], *Sebastien Schaefer*[‡], *Angela Sanchez-Sanchez*[‡], *Alain Celzard*[‡], *Vanessa Fierro*[‡]*, *M. Mercedes Maroto-Valer*[†], *Susana García*[†]*

[†] Research Centre for Carbon Solutions (RCCS), School of Engineering and Physical Sciences, Heriot-Watt University, Edinburgh EH14 4AS, United Kingdom

[‡] Université de Lorraine, CNRS, IJL, F-88000 Epinal, France

ABSTRACT

Activated carbons (ACs) are among the most commonly used sorbents for CO_2 capture because of their high surface areas and micropore volumes, which depend on precursor and activation methods. In this study, we evaluated different ACs obtained from a low-value fraction of liquid-derived coal pyrolysis, namely phenolic oil, which was used as gel precursor before carbonization and KOH activation. CO_2 capture performances were determined at temperatures between 25 and

120°C, with CO_2 concentrations ranging from 5 to 90 vol. %. The most efficient sample captured 2.86 mmol of CO_2/g AC at 25°C and 1 bar, which is a highly competitive capture capacity, comparable to previously reported values for ACs without any modification/functionalization. Finally, their thermal stability and cyclability (i.e., for a minimum of six adsorption-desorption cycles) were evaluated. CO_2 uptake was not affected by desorption temperature after six adsorption-desorption cycles. Based on the results obtained in this work, the role of the textural properties into the CO_2 capture at realistic postcombustion temperatures and partial pressures was elucidated. In particular, we concluded that CO_2 adsorption performance was more related to the volume of the narrowest pores and to the average pore size than to the surface area.

KEYWORDS: Coal tar; Xerogels; Cryogels; Activated carbon; Pore Texture; Post-combustion CO_2 capture.

1. Introduction

Atmospheric CO_2 concentration is continuously increasing, reaching values higher than 414 ppm in June 2019 [1]. To reduce this concentration, one of the key actions agreed is the application of Carbon Capture and Storage technologies (CCS) according to the report of the Intergovernmental Panel on Climate Change (IPCC) [2].

Among the various carbon capture technologies, the use of solid adsorbents is becoming more relevant because of several advantages, such as lower energy requirements during regeneration and increased stability under corrosive atmospheres, compared to absorption-related processes [3-5]. However, these solids need to meet specific requirements to be considered for adsorption-based carbon capture processes including: 1) low heat capacity, 2) fast kinetics, 3) high CO_2

capture capacity, 4) thermal and chemical stability, 5) high CO_2 selectivity, 6) long service life, and 7) low-cost raw materials [6,7].

Various activated carbons (ACs), zeolites, ordered mesoporous silica, metal-organic frameworks (MOFs) and porous organic polymers (POPs), have been already evaluated for CO_2 physical adsorption [5,8], as well as amine-based solids for CO_2 chemical adsorption [7].

Even though amine-based solids present lower heat capacity than liquid absorbents, chemical adsorption is associated with high costs and low CO_2 capture capacities compared to physical adsorption [7]. For this reason, an increasing number of studies have focused on using porous solids for physical adsorption-based processes. Among them, CO_2 adsorption with ACs offers one the most promising alternatives due to their low cost, high stability after a large number of cycles, easy production, high surface area, and cheap regeneration after CO_2 capture [9,10].

ACs are produced by physical or chemical activation of carbon precursors, which can be coals [11-13], various pyrolized materials [14-16], or biomass [17-20]. In any activation process, the ultimate goal is to increase the textural properties of the material (i.e., surface area and pore volume). Physical activation requires CO_2 or steam at high temperatures (≥ 800ºC), while chemical activation requires impregnation or blending of the precursor with an activating agent (i.e., H_3PO_4 or KOH, among others) and heated to lower temperatures than those used for physical activation [5,15].

Wang et al. proved that CO_2 capture capacity is directly proportional to the micropore volume for ACs having similar BET surface areas, and demonstrated that both high surface area and high porosity are needed to increase the CO_2 capture on ACs [21]. Lee et al. [8] and Sevilla et al. [22] showed that the CO_2 capture capacity is directly related to the presence of ultramicropores (pore diameter < 0.7 nm) and supermicropores (pore diameter 0.7-2 nm). Furthermore, Lee et al. also concluded

that the pore size distribution (PSD) of micropores narrower than 0.7 nm has a high influence on the CO_2 capture capacity [8], in agreement with Marco-Lozar et al. who showed that the CO_2 capture takes place in the ultramicropores at low partial pressures and at 25ºC [23].

Carbon gels are known as materials with a highly developed porous texture [24], and are usually produced by the pyrolysis of organic and dried resorcinol-formaldehyde (RF) [24] or phenol-furfural [25] gels. Once the pyrolysis of the gel is controlled, it is possible to obtain highly microporous carbons, essentially comprising pores narrower than 1.5 nm. Robertson and Mokaya thus obtained ACs from RF carbon gels with micropores of size mainly between 0.8 and 1.2 nm, and measured CO_2 adsorption capacities of 2.7 to 3 mmol/g at 25ºC [26]. However, resorcinol and phenol are expensive and this has a direct impact on the final cost of carbon gels. Hence, new low-cost precursors should be targeted and studied to obtain highly microporous activated carbons for CO_2 capture applications. Furthermore, no assessment of the role of the ACs pore texture on the CO_2 adsorption process under more realistic operational capture conditions has been reported and could provide very helpful insights for future developments targeting improved AC materials.

In this study, we evaluated the CO_2 capture performance, at realistic operating temperatures, of carbon xerogels and cryogels based on low-value phenolic oil derived from coal pyrolysis. Furthermore, CO_2 adsorption studies were conducted at CO_2 concentrations (5 – 30 vol. %) representative of different flue gas streams from power plants or industries [27, 28]. Selected ACs were submitted to a cyclic study to evaluate the effect of the regeneration temperature on the carbon stability and on their CO_2 uptake over several adsorption/desorption cycles. Finally, CO_2 capture capacities at different temperatures were correlated with the pore texture, and clear relationships were obtained.

2. Experimental

2.1 Activated carbons

2.1.1 Synthesis

Three activated carbon (AC) series: XiPPO, XPPO and CWPO were prepared as indicated in Table 1. The first letter of the materials label stands for the type of gel (i.e., X for xerogel and C for cryogel). The organic gels used as AC precursors were prepared by dissolving phenolic oil (PO) and formaldehyde either in isopropanol (i) for XiPPO, in n-propanol (-) for XPPO, or in water (W) for CWPO series of gels. Acidic catalysis, using para-toluenesulphonic acid, was used in the synthesis of the XiPPO series, and basic catalysis, using NaOH, was used in the synthesis of the XPPO and CWPO ones.

After gelation in their respective solvent, the resultant wet hydrogels or alcogels were dried by convective heat exchange (85°C, 12h) in the case of XiPPO and XPPO materials, and by freeze-drying in the case of the CWPO series. Prior to the freeze-drying process of the CWPO hydrogels, water was exchanged thoroughly by tert-butanol (35°C, one exchange per day for 3 days).

Table 1. Preparation methodology of the samples.

Series of samples	XiPPO	XPPO	CWPO
Type of gel	Xerogel	Xerogel	Cryogel
Organic precursor	Phenolic oil	Phenolic oil	Phenolic oil
Solvent used	isopropanol	n-propanol	Water
Type of Catalysis	Acidic	Basic	Basic
Activation agent	KOH	KOH	KOH

The dried gels were then ground and mixed with KOH, using KOH/dried gel mass ratios of 3, 4 and 5 for XiPPO, of 1, 2, 3, 4 and 5 for XPPO, and of 1, 2, 3 and 4 for the CWPO series. Chemical activation of the dried gel was next performed by heating the KOH/dried gel mixture up to 750ºC, and maintaining the final temperature for 1h in nitrogen flow (100 mL/min). Thus, pyrolysis and chemical activation were carried out in one single step. The obtained ACs were finally washed with 1 mol/L HCl, subsequently washed with distilled water in a Soxhlet extractor for 5 days, and dried in a ventilated oven (105ºC, 12h). The ACs were labelled by adding the KOH/gel mass ratio (i.e., from 1 to 5) to the name of their gel precursor. Thus, for instance, XiPPO_3 is an activated carbon prepared from a xerogel synthesized with isopropanol as solvent, dried by convection, ground and activated with a KOH/gel mass ratio equal to 3.

For the sake of comparison, two well-known commercial ACs from Kansai Coke and Chemicals Co. Ltd (i.e., MSP-20X and MSC-30) were also characterized and tested as CO_2 adsorbents.

2.1.2 Textural characterisation

Textural characterization was performed by nitrogen and carbon dioxide adsorption at -196°C and 0°C, respectively, using an automatic adsorption apparatus (ASAP 2020, Micromeritics). Adsorption data were treated using the Microactive® software from Micromeritics. Prior to gas adsorption, all samples were degassed under secondary vacuum at 110°C until the pressure stabilized at about 0.2-0.4 mPa for more than 48h. Further degassing was carried out at the measuring port for at least 6h. Cool and warm volumes were determined after nitrogen or carbon dioxide adsorption to avoid helium entrapment in the narrowest pores.

The BET area calculated by the Brunauer-Emmett-Teller (BET) method [29], A_{BET}, was obtained by applying the BET equation in the appropriate range of relative pressures [30]. A_{BET} was only

determined for comparing our results with those reported in the open literature, and not used here for further calculation because of the well-known overestimation of surface area when applying the BET equation to materials having highly developed supermicroporosity. Micropore volumes were obtained using the Dubinin-Radushkevich (DR) equation [31], and they are again only given here for comparison purposes with the literature [32, 33]. The DR method was applied both to N_2 (-196°C) and to CO_2 (0°C) adsorption isotherms to obtain $V_{DR,N2}$ and $V_{DR,CO2}$, respectively. The pore size distributions (PSDs) were obtained by using the non-local density functional theory (NLDFT) from the Solution of Adsorption Integral Equation Using Splines (SAIEUS®) routine. This method has the advantage of combining both CO_2 and N_2 adsorption data to get more accurate PSDs [34]. Moreover, it allows fitting the PSDs with a spline model, avoiding the usual singularities of the classical DFT model. The average micropore diameter was calculated using this PSD, $L_{0,NLDFT}$, and also the by applying the DR method together with the Stoeckli equation [35], $L_{0,DR}$. The mesopore volume was calculated by subtracting the micropore volume obtained from the NLDFT method, $V_{mic\ NLDFT}$, to the total pore volume directly measured by N_2 adsorption at a relative pressure of 0.99. The NLDFT method was also used to determine the surface area, S_{NLDFT}, by integrating the PSDs over the whole range of pore sizes [36]. Moreover, the pore volumes corresponding to pore widths below 0.5 nm ($V_{L<0.5}$), below 0.7 nm ($V_{L<0.7}$), between 0.7 and 2 nm ($V_{0.7<L<2}$), below 2 nm ($V_{L<2}$) and between 2 and 50 nm ($V_{2<L<50}$), were also determined by integrating the PSD over the relevant pore diameters.

2.2 CO_2 capture evaluation

The CO_2 capture capacities were determined using a TA Q500 thermogravimetric analyzer (TA Instruments). In all experiments, a platinum pan was filled with approximately 8 mg of the AC to

be tested. The pan was heated up to 120ºC and kept at this temperature for 30 minutes under N_2 flow (100 mL/min) to eliminate pre-adsorbed gases or water from the AC surface. After drying, the desired temperature (25, 50, 75, 100, or 120ºC) was reached and the sample was kept under nitrogen flow until constant weight. Once the steady state was reached, the N_2 flow was switched to a total of 100 mL/min flow with a 90 vol. % of CO_2 in N_2, and the temperature was maintained for 30 minutes to ensure that the total CO_2 capture capacity was achieved. CO_2 adsorption at 25ºC was repeated at least 3 times to evaluate the deviation and repeatability of the capture capacity for each AC, and the materials presenting the highest CO_2 capacity were selected for further studies.

For the most efficient ACs, the capture capacity at 25ºC and at different concentrations of CO_2, from 5 to 90 vol. % in N_2, was evaluated. Low values such as 5, 15, 18 and 25 vol. % are particularly interesting to mimic the behavior of ACs in the presence of common concentrations of CO_2 from the combustion of natural gas and pulverized coal [27]. Furthermore, we used the best sample of the XiPPO series to evaluate the ageing of the AC after six adsorption-desorption cycles. For this purpose, we carried out adsorption at 25ºC using a pure CO_2 flow of 100 mL/min and, after desorption, the AC was regenerated at different temperatures (i.e., 125, 150, 175 or 200ºC). Moreover, a thermal stability study was carried out for each sample for evaluating its behavior from 25 to 220ºC with a heating ramp of 10ºC/min under a 100 mL/min flow of inert atmosphere. Finally, six cycles of adsorption-desorption were done for the best sample selected out of each family of AC, using 200ºC as regeneration temperature.

3. Results and discussion

3.1 Porous texture of the ACs

Table 2 shows the main textural parameters of the ACs considered in this study. All were essentially microporous, with micropore fractions ranging from 60 to 95 %, and with a well-developed A_{BET}, from 1356 to 3305 m^2/g. S_{NLDFT} gives a more realistic determination of the surface area (having in mind that the maximum surface area of an AC is 2630 m^2/g [37]), and it indeed varied from 1436 to 2216 m^2/g. Average micropore size, $L_{0,\,NLDFT}$, ranged from 0.7 to 1.3 nm. The two commercial ACs from Kansai, labelled according to their commercial denomination, MSC-30 and MSP-20X, had porous textures that compared very well with those of the present experimental activated carbon gels, whether surface areas or pore volumes are considered. This is an important result, since it should be recalled that the present materials were derived from a poorly valorized industrial waste: phenolic oil.

Table 2. Textural properties of all activated carbons.

Sample	A_{BET}	S_{NLDFT}	V_{tot}	$V_{L<0.5}$	$V_{0.5<L<0.7}$	$V_{L<0.7}$	$V_{0.7<L<2}$	$V_{2<L<50}$	$V_{DR,\,N2/CO2}$	$L_{0,\,NLDFT}$	$L_{0,\,DR}$ (N_2)
	m^2/g	m^2/g	cm^3/g	cm^3/g	cm^3/g	cm^3/g	cm^3/g	cm^3/g	cm^3/g	nm	nm
MSP-20X	2363	2007	0.93	0.02	0.17	0.19	0.69	0.05	0.83/0.42	1.04	0.96
MSC-30	3305	2216	1.60	0.00	0.04	0.04	0.91	0.64	1.02/0.37	1.28	1.29
XiPPO_3	2694	2086	1.15	0.01	0.14	0.15	0.80	0.19	0.90/0.44	1.16	1.21
XiPPO_4	2967	2133	1.34	0.01	0.10	0.11	0.85	0.38	0.94/0.41	1.23	1.25
XiPPO_5	2494	1913	1.11	0.02	0.08	0.10	0.76	0.25	0.83/0.47	1.18	1.24
XPPO_1	1364	1494	0.56	0.03	0.25	0.28	0.25	0.03	0.52/0.53	0.81	0.72
XPPO_2	1848	1943	1.10	0.02	0.13	0.15	0.73	0.22	0.82/0.39	1.19	1.25
XPPO_3	2729	2036	1.23	0.02	0.09	0.10	0.81	0.32	0.90/0.46	1.20	1.27
XPPO_4	2673	1964	1.27	0.02	0.07	0.10	0.75	0.42	0.85/0.36	1.23	1.30
XPPO_5	2383	1713	1.14	0.01	0.06	0.08	0.67	0.39	0.76/0.39	1.25	1.33
CWPO_1	1356	1436	0.56	0.03	0.22	0.25	0.27	0.04	0.51/0.41	0.85	0.80
CWPO_2	2245	1907	0.99	0.02	0.15	0.17	0.69	0.13	0.79/0.43	1.14	1.15
CWPO_3	2551	2039	1.21	0.02	0.11	0.13	0.79	0.28	0.87/0.42	1.21	1.20
CWPO_4	2607	2027	1.30	0.02	0.09	0.11	0.77	0.42	0.87/0.39	1.24	1.24

3.2 CO_2 capture capacities at 25ºC

3.2.1 General trends

Figure 1 shows the CO_2 capture capacity, in mmol of CO_2 per gram of adsorbent, of each AC measured at 25ºC. The best samples of each series were XPPO_1 > CWPO_1 > MSP-20X > XiPPO_3. Table S1 shows the average CO_2 capture capacity of all samples after three repetitions. The deviation in the CO_2 adsorption measurement was calculated for all samples, and the CO_2 capture capacities were very repeatable, with a relative error of less than 3%.

XPPO_1 had the highest CO_2 capture out of all samples, 2.86 mmol CO_2/g, followed by CWPO_1, 2.66 mmol CO_2/g. In the XPPO series, the XPPO_1 presented a lower A_{BET} than the rest, but a much higher fraction of micropores (> 90 %) as well as a higher volume of narrow pores (V_{DR}). These values are comparable with previous work evaluating the use of asphalt as precursor of activated carbons [38].

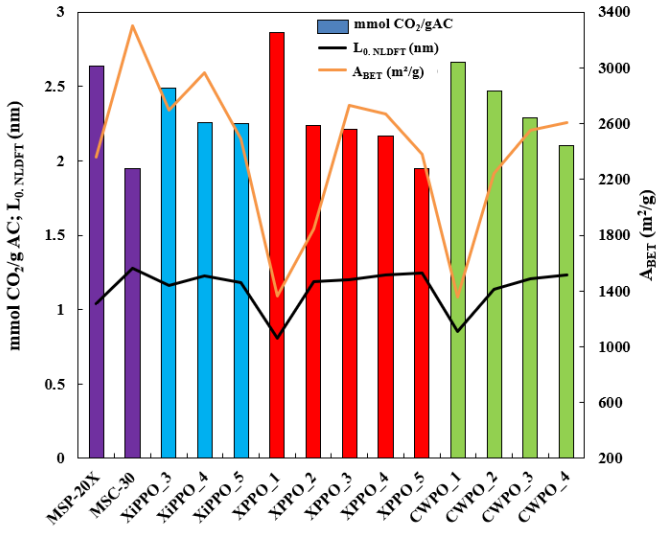

Figure 1. Average micropore size $L_{0,\ NLDFT}$ (black line), A_{BET} (yellow line) and CO_2 capture capacity (mmol/g AC) of each activated carbon. (Purple for KANSAI, blue for XiPPO, red for XPPO group and green for CWPO).

The CO_2 capture capacity of samples XPPO_2, XPPO_3 and XPPO_4 slightly decreased as the xerogel/KOH mass ratio increased because the micropore volume fraction decreased, which implied a lower CO_2 capture capacity. The same trend was observed for the XiPPO samples, XiPPO_3 presenting the highest CO_2 capture capacity and XiPPO_4 and XiPPO_5 having similar CO_2 capture capacities, with different textural characteristics. The latter clearly implies that CO_2 capture can be maintained even if the micropore volume decreases, as long as the total pore volume of the activated carbons increases sufficiently because CO_2 capture is due to both adsorption and pore filling.

Otherwise, for the CWPO and Kansai samples, a clear trend could be observed, as the decrease in CO_2 capture capacity appeared constant as the degree of activation increased (related to the cryogel/KOH ratio in the case of CWPO). In both families of materials, the samples that were more activated had an increase of surface area but that was not enough to compensate the decrease of CO_2 capture capacity, related to the correspondingly lower microporous fraction and micropore volume. MSP-20X and MSC-30 indeed had microporous fractions of 96.80% and 59.83 %, respectively, and surface areas of 2363 m^2/g and 3305 m^2/g, respectively.

Finally, comparing in all cases the best samples from each family, it was observed that the samples with the highest $V_{0.5<L<0.7}$ and the lowest $L_{0,\,NLDFT}$ were the ones with the highest CO_2 capture capacity.

More generally, the adsorption of CO_2 near room temperature and atmospheric pressure is mainly due to the narrowest micropores. A quite good linear correlation between the ultramicroporous volume ($V<0.7$) and the amount adsorbed was indeed found ($R^2 = 0.89$). It highlights the importance of such narrow pores when a good CO_2 capture under these conditions is sought (Figure 2a), which corroborates what has been previously reported [14, 39, 40].

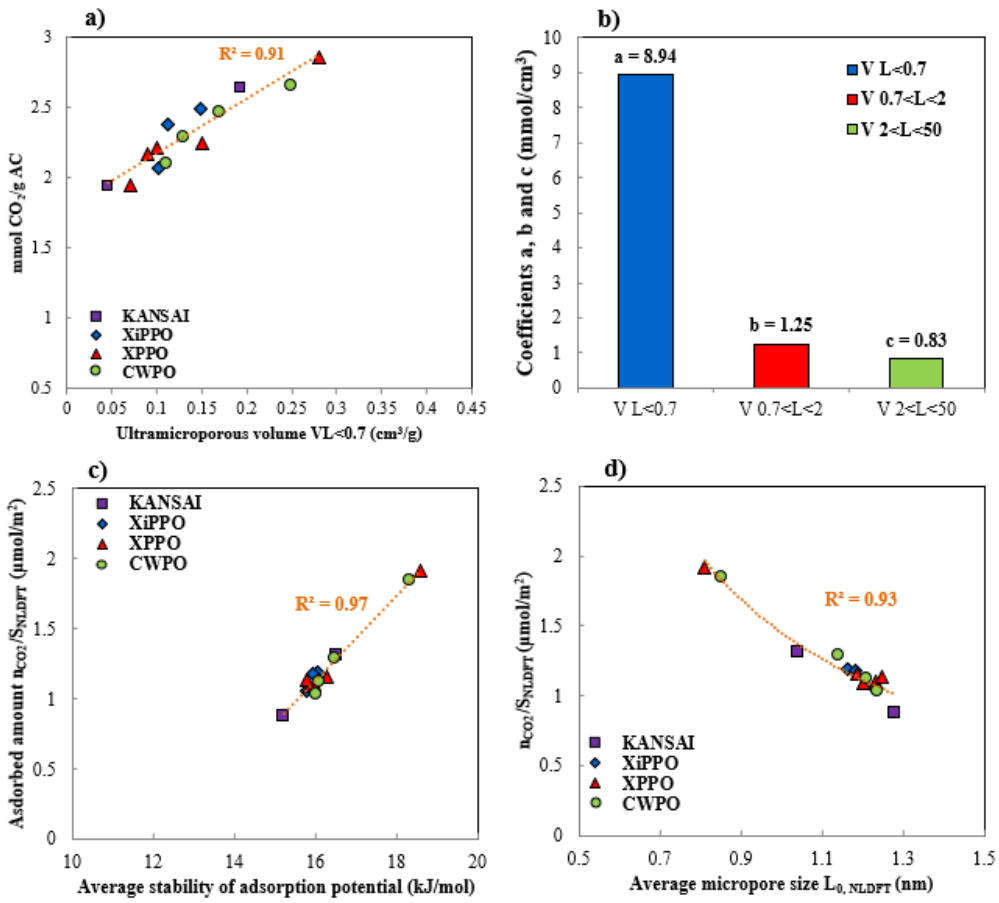

Figure 2. a) Adsorbed CO_2 amount at 25ºC as a function of the ultramicroporous volume. b) Coefficients of multiple linear regressions for CO_2 adsorption at 25°C. c) Amount adsorbed per unit of surface area as a function of the average adsorption potential stability (25°C and 1 bar). d) Same as c) but versus $L_{0,\,NLDFT}$. The dotted lines are just guides for the eye.

3.2.2 Pore size effect: Multiple linear regression

In order to highlight the relative importance of pore size, some authors suggested to perform a multiple linear regression taking into account the pore volumes for each class of pores ($V_{<0.7}$, $V_{0.7<L<2}$ and $V_{2<L<50}$) and the corresponding adsorbed amount of gas, n_{ads} (T,P) [41,42]. The equation of this multiple linear regression takes the following form (eq. 1):

$$n_{ads}\,(T,P) = a\,(T,P).V_{L<0.7} + b\,(T,P).V_{0.7<L<2} + c(T,P).V_{2<L<50} \qquad \text{(eq. 1)}$$

$V_{L<0.7}$, $V_{0.7<L<2}$ and $V_{2<L<50}$ refer to ultramicroporous, supermicroporous and mesoporous volumes, respectively, whereas a, b and c are real numbers and are the coefficients of the multiple linear regressions. The fitting algorithm (Levenberg-Marquardt) led to a good regression ($R^2 = 0.87$), while the p-value was far below 0.05 (i.e., ≈ 0). The high value of a compared to b and c, 8.94, 1.25 and 0.83 mmol/cm^3, respectively, showed that the ultramicropore volume is of paramount importance for the adsorption of CO_2 at 25°C (Figure 2b).

This conclusion is further confirmed by the evolution of such coefficients as a function of the pore size of the corresponding pore classes, which exhibits a dramatic decrease as the pore size increases. Figure S1 shows the same trend but when the ultramicroporous volume ($V_{L<0.7}$) is subdivided into two other pore classes ($V_{L<0.5}$ and $V_{0.5<L<0.7}$). In this case, the coefficients of the multilinear regression show a dramatic and exponential-like decay as the pore size increases.

3.2.3 Adsorption potential

The adsorption potential decreases as the pore size increases due to less overlap of the interaction potentials exerted by the facing pore walls. Thus, pores having a size less than 0.7 nm and, to a higher extent, pores narrower than 0.5 nm have a paramount influence on the ability of materials to adsorb CO_2 at low pressure (1 bar) and at room temperature [14].

These trends are also confirmed by the simple linear regression presented in Figure S2.

In order to verify this, the adsorption potential was modelled using the well-known Steele potential [43]. The parameters selected for the modelling were the same as those used by Kurniawan et al. for Grand Canonical Monte Carlo modelling of gas adsorption [44].

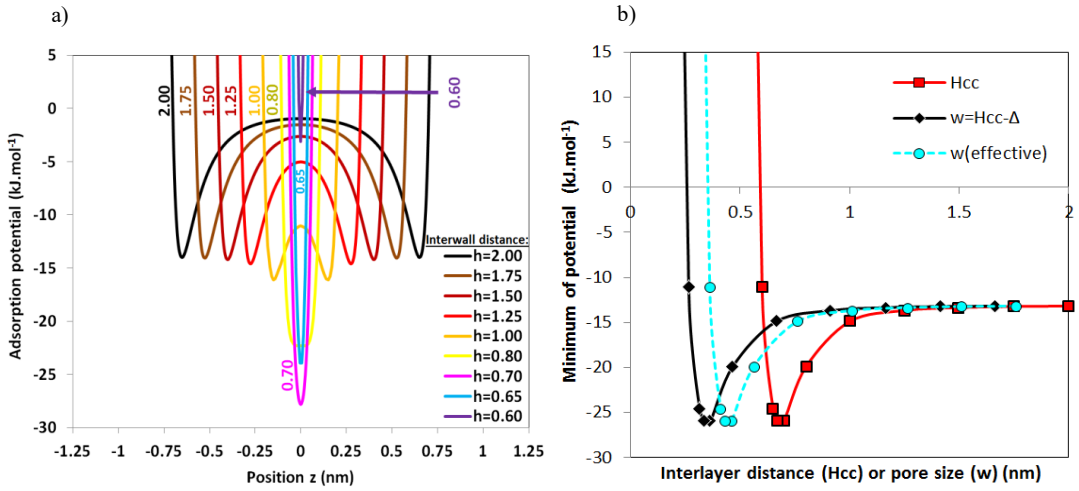

Figure 3. Steele adsorption potential for the CO_2 – graphite system (slit pores model).

The adsorption potentials, as well as their related minima, are reported in Figure 3, where the Steele adsorption potential and the minimum of Steele's potential as a function of the distance between median planes of the graphitic pore walls are represented.

This Steele potential [43] is described by the following expression (eq. 2):

$$U_{sf}(z) = 2.\pi.\rho_s.\epsilon_{sf}.\sigma_{sf}.\Delta.\left[\frac{2}{5}.\left(\frac{\sigma_{sf}}{z}\right)^{10} - \left(\frac{\sigma_{sf}}{z}\right)^{4} - \frac{\sigma_{sf}{}^4}{3.\Delta(0.61\Delta+z)^3}\right] \qquad \text{(eq. 2)}$$

where ρ_s is the number of atoms per unit volume of graphite (114 nm^{-3}), Δ is the interlayer spacing of graphite (0.335 nm), z is the distance to the graphite wall, ϵ_{sf} and σ_{sf} are the Lennard-Jones parameters for the CO_2 molecule in interaction with graphite. The values of these parameters were obtained using the classical Lorentz-Berthelot combination rules for pure fluid (CO_2) and solid (graphite). For the CO_2-graphite system and in the case of one-center model, the parameters were approximated to $\epsilon_{sf} / k_b = 82.3165\,\mathrm{K}$ and to $\sigma_{sf} = 0.35075(\mathrm{nm})$ [44]. Ravikovitch et al. previously proposed a similar approximation for DFT modelling [45]. The total adsorption in a medium, confined between two walls of a slit pore, reads (eq.3):

$$U_{sf-total}(z) = U_{sf}(z) + U_{sf}(H_{cc} - z) \qquad \text{(eq. 3)}$$

where H_{cc} is the centre-to-centre distance, or distance between the median planes of the graphitic walls (Å). Then, the potential can be converted from K to kJ/mol using Avogadro and Boltzmann constants.

As used by some authors, an indicator of the strength of the potential is its stability, (s) [46]. The stability of a potential is defined by the opposite value of the minimum of the potential in a valid range of z (eq. 4).

$$s(H_{cc}) = -\min(U_{sf-total}(z, H_{cc})) \quad \text{(eq. 4)}$$

The adsorption potentials, as well as their related minima, are reported in Figures 3. It can be noticed that the adsorption potential follows a nonlinear evolution as a function of the distance between the two graphite walls. This adsorption potential decreases down to almost -28 kJ/mol for H_{cc} = 0.7 nm. Such distance corresponds to the space between the median planes of the wall. Given that the interlayer spacing in graphite is 0.335 nm, this distance corresponds to a real pore size of 0.365 nm for this lowest minimum of potential [46]. Indeed, the effective pore size can be calculated from the interplanar (H_{cc}) distance.

The interlayer distance of pure and defect-free graphite (Δ) is equal to 0.335 nm. Thus, the effective pore size can be calculated using the following formula. (eq. 5):

$$w = H_{cc} - \Delta \quad \text{(eq. 5)}$$

Some authors suggested that this calculation method leads to a poor estimation of the effective pore size [47,48]. Consequently, they proposed to use another estimation (eq. 6).

$$w_{effective} = H_{cc} - (2.z_0 - \sigma_{ff}) \quad \text{(eq. 6)}$$

where z_0 has the following expression (eq. 7):

$$z_0 = 0.8506.\sigma_{Sf} \quad \text{(eq. 7)}$$

Above $H_{cc} \approx 1.00$ nm (i.e., for an effective pore size $w_{effective}$ equal to 0.76 nm), the minimum of adsorption potential is almost constant and asymptotically converges to a value close to 13.95 kJ/mol. Thus, in pores wider than ultramicropores, CO_2 is assumed to adsorb in the same way as that occurring on a flat graphitic surface. According to these observations, based on the minimum of adsorption potential, the ideal pore size for CO_2 adsorption would be close to 0.45 nm ($H_{cc} \approx 0.7$ nm). However, in practice, some authors have reported that cooperative adsorption, occurring in pores wider than 0.6 nm, promotes high densities of adsorbed CO_2 as the pressure increases [46].

Representing the adsorbed amount per unit of surface area (using S_{NLDFT}) as a function of the average potential stability (Figure 2c) makes the cloud of points much narrower compared to the case of using the average micropore size (Figure 2d), which is discussed in the next subsection.

3.2.4 Influence of adsorption potential and porous texture on CO_2 capture capacity

The amount of adsorbed CO_2 per surface area ($\mu mol.m^{-2}$) is presented in Figure 2d versus the average micropore size. This methodology and representation have been already used by several authors [49,50]. Representing the adsorbed CO_2 per surface area versus A_{BET} and $L_{0\,DR,N2}$, a good fit was also obtained ($R^2 = 0.86$, Figure S3) but the quality of the fit was far better when using S_{NLDFT} and $L_{0,\,NLDFT}$ (i.e., $R^2 = 0.93$) (Figure 2d).

Likewise, the BET and DR methods overestimate the surface area and the micropore volume, respectively, of highly activated carbons. The linear dependence of the adsorbed amount of CO_2 per unit of surface area as a function of the average stability of the adsorption potential (Figure 2c) induces a curvature when the same quantity is observed as a function of the average micropore size (Figure 2d). Indeed, the stability of the adsorption potential has a highly non-

linear dependence with the pore size (Figure 3b) which induces this curvature. With the exception of commercial activated carbons (MSC-30 and MSP-20X), all data points are located on one single trend line (Figure 2d). This suggests that the shapes of the pore size distributions of activated carbons derived from phenolic oil are similar or, at least, do not have, in this particular case, a significant influence on the adsorbed density. Moreover, Figure S4 confirms the similarity of the pore size distributions of activated carbons derived from phenolic oil. Indeed, the three families of synthesized materials follow the same trends: for each pore fraction, each class of pores depends on $L_{0,NLDFT}$ in a similar way. The KANSAI family is the only one to present, here, some differences in the shape of the pore size distributions (Figure S4). Indeed, the MSP-20X has, given the average size of its micropores, a lower ultramicroporous volume than the rest of the materials. Hence, the advantage of using average adsorption potential stability (Figure 2b) instead of average micropore size (Figure 2c) is both to reduce scattering when comparing different families of materials and to linearize the trend.

3.3 CO_2 capture capacity above room temperature (50-120°C)

As it has been confirmed previously, the narrow micropore volume is the most important parameter for CO_2 capture at low temperatures, also concluded by Sevilla et al.[51]. However, in combustion processes, the most common flue gas temperatures range from 50 to 120°C [3, 52]. Figure 4 shows the CO_2 uptake for the best samples previously identified (MSP-20X, XiPPO_3, XPPO_1 and CWPO_1) for a representative range of temperatures from 25 to 120°C. As expected, the CO_2 capture capacities of all samples decreased as the adsorption temperature increased, because CO_2 physisorption is an exothermic process.

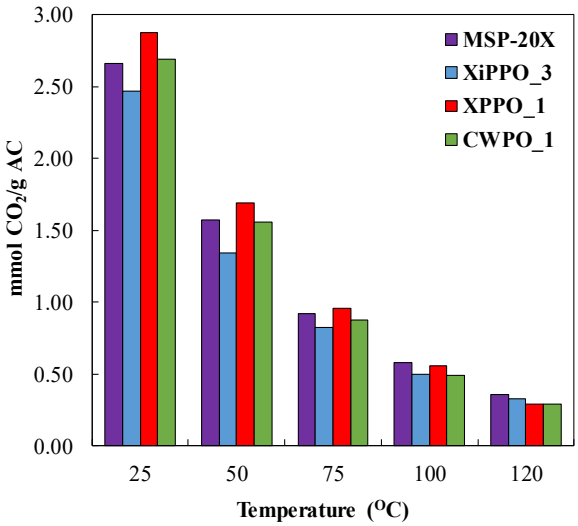

Figure 4. CO_2 capture capacity of the most efficient samples as a function of adsorption temperature. (Purple for MSP-20X, blue for XiPPO_3, red for XPPO_1 and green for CWPO_1).

In agreement with Serafin et al. [14], as the adsorption temperature increases, the range of pore size in which the capture of CO_2 mostly takes place is considerably reduced and pores narrower than 0.5 nm become more important. However, it was observed that at 120°C, the CO_2 capture capacity of all samples were very similar. Indeed, the CO_2 uptake of XPPO_1 was the lowest, even though it had the highest volume of narrow pores and the lowest $L_{0,NLDFT}$. Hence, as the capture temperature increases, the micropore volume of the samples becomes less relevant, as opposed to the surface area and the total pore volume which become more important.

Indeed, the higher the specific area and total pore volume the higher the density (per mass unit of carbon material) of possible defects on the surface of carbon structure (i.e. surface groups, edges, corrugation and other topological defects). Under high temperature (i.e. 120 °C), such defects should have a greater importance than under lower temperatures due to the polarization effect

they induce on the CO_2 molecules. This statement is justified by the study of adsorption enthalpies as detailed below.

The calculation of adsorption enthalpies using Henry's law is detailed in the supplementary information. The linear fits had a high R^2 (> 0.97). The enthalpies of CO_2 adsorption on the materials MSP-20X, XiPPO_3, XPPO_1 and CWPO_1 are respectively equal to 20.2, 20.1, 24.5 and 23.9 kJ/mol. These values are in the typical range of CO_2 adsorption on activated carbons [53, 54]. The decrease in heat of adsorption (opposite of the enthalpy of adsorption) as the average micropore size increases (Figure 5a) is due to the decrease of the adsorption potential.

When the heat of adsorption is represented in relation to the average stability of the adsorption potential calculated previously, instead of the average size of the micropores, the trend becomes perfectly linear but does not correspond to the identity function (Figure 5b).

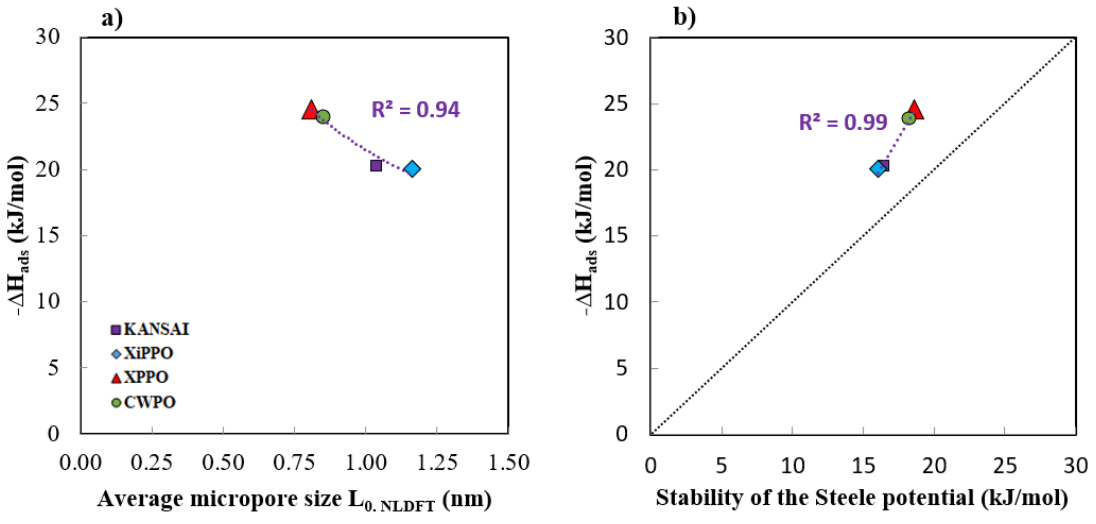

Figure 5. Heat of adsorption as a function of a) average micropore size according to NLDFT, and b) stability of the adsorption potential.

This non-equality might be due to the fact that the potential of adsorption does not perfectly reflect the substrate-adsorbate interactions. Indeed, the adsorption potential does not account for intermolecular or lateral interactions of the adsorbate. These could increase the apparent heat of adsorption. In addition, the small amount of CO_2 possibly subjected to cooperative adsorption in the larger micropores could also affect the heat of adsorption and induce a higher heat of adsorption. Moreover, the adsorption potential has been calculated for an infinite flat graphitic surface, thus without edges or corrugation, and in the absence of specific surface group that might experimentally affect the adsorption heat and the adsorption process. Such characteristics of the carbon surface (corrugation, defects, edges and surface groups) could explain the higher values of adsorption heat obtained experimentally, compared to the average stability of adsorption potential.

Figure 6a shows the evolution of the heat of adsorption as a function of temperature and average micropore size. The heat of adsorption increases as the temperature of adsorption increases due to the preferential filling of the smallest pores at high temperature. Indeed, the high temperatures induce a greater decrease in the density of the adsorbed layer in the wide pores than in the narrow pores where the adsorption potential is very high [14]. In addition, the increase in temperature gives more importance to strong polarized adsorption on the surface of the sorbent compared to physisorption. In general, defects in carbon structure itself or surface groups such as hydroxyls can induce such strong polarized adsorption phenomena [55, 56].

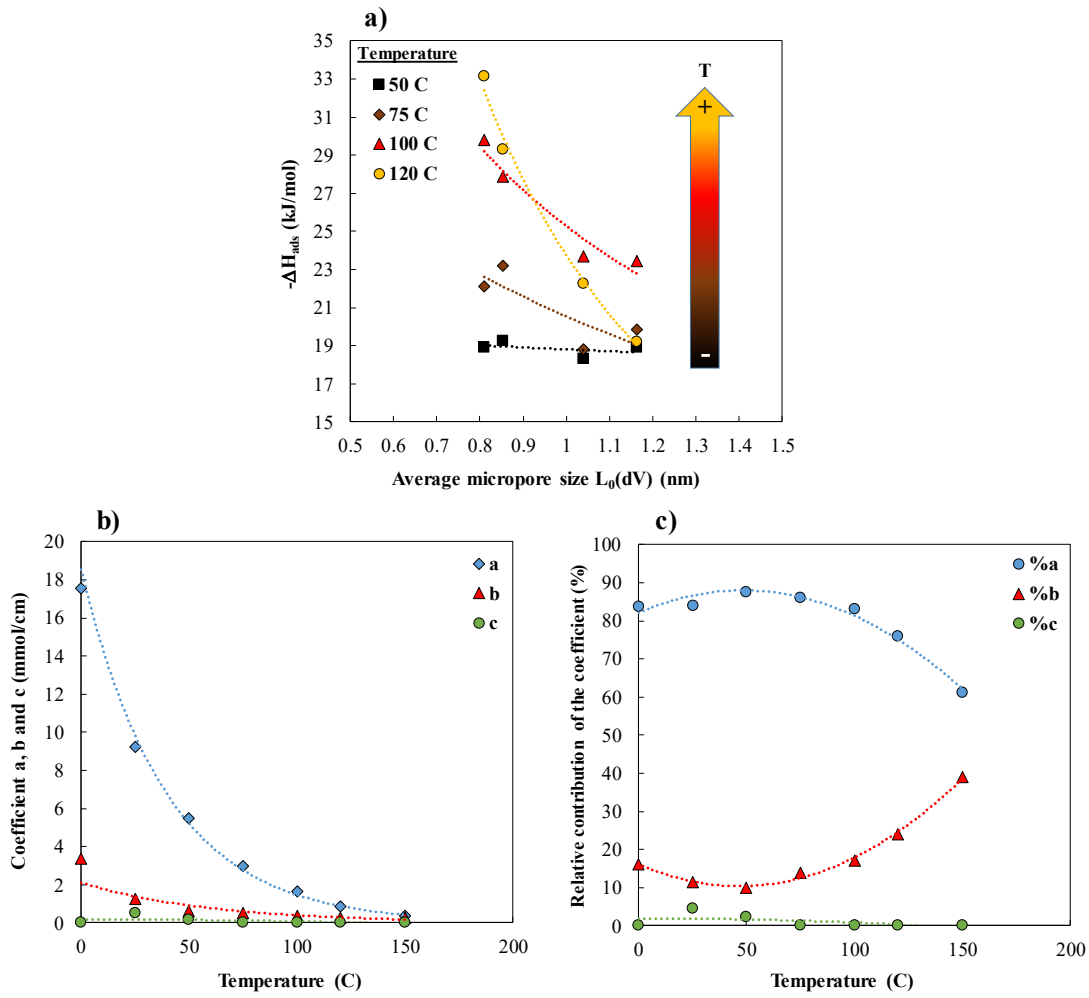

Figure 6. a) Heat of adsorption as a function of the average micropore size for different temperatures, b) Coefficients *a*, *b* and *c* of the multilinear regression (eq. 1), and c) their relative contribution as a function of temperature.

By applying multiple linear regression (eq. 1) to each adsorption temperature, the coefficients a, b and c, corresponding to the contributions (in mmol/cm^3) to CO_2 adsorption for each pore size, have been calculated. The variation of these coefficients as well as their relative contributions to capture capacities are shown in Figure 6b and 6c, respectively, as a function of temperature. The ultramicropores always constituted the most important volume fraction (Figure 6b), although their importance approached that of supermicropores at 120°C (Figure 6c).

Figure 6b exhibits an exponential decay of all coefficients related to the negative effect of temperature on the physisorption process. In addition, the relative contribution of each pore size (Figure 6c) shows that, in a range close to room temperature (i.e., 25-75°C), the contribution of ultramicropores increases (coefficient a) while that of supermicropores (coefficient b) decreases, which is due to the higher adsorption potential in ultramicropores. In contrast, above 75°C, the contribution of supermicropores (coefficient b) begins to increase. This indicates that the surface becomes, above a given temperature, more attractive for the adsorption of CO_2.

3.4 Effect of partial CO_2 pressure on the capture capacity

When transforming fossil fuel energy in any combustion plant, the concentration of CO_2 released into the atmosphere is between 5 and 30 vol. %: the most common values from pulverized coal fired plants ranges from 8 to 15 vol. % [28], whereas the concentration can reach 30 vol. % with cement plants [27].

Figure 7 shows the CO_2 adsorption at 25°C for the most efficient samples of each family (MSP-20X, XiPPO_3, XPPO_1 and CWPO_1) at different partial pressures of CO_2. It was observed that at low concentrations, 5, 15 and 18 % by volume, the CO_2 capture capacities of MSP-20X and XiPPO_3 were similar, with a higher CO_2 uptake of CWPO_1.

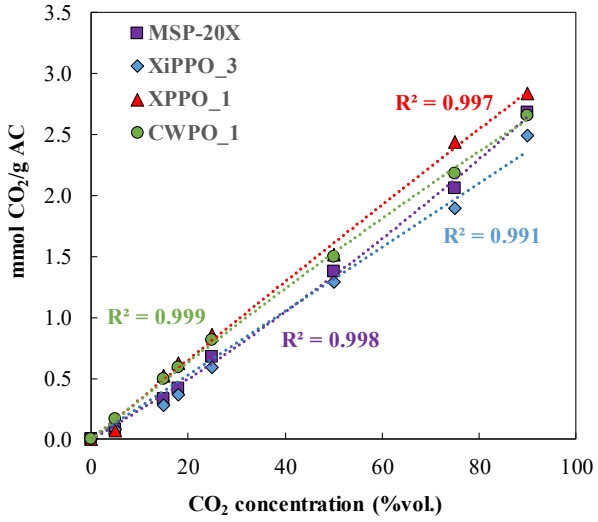

Figure 7. CO_2 capture capacities at 25ºC for the most efficient samples as function of the CO_2 concentration. (Purple for MSP-20X KANSAI, blue for XiPPO_3, red for XPPO_1 and green for the CWPO_1).

The CO_2 capture of XPPO_1 at 5 vol. % of CO_2 was the lowest among all samples. However, it became the highest as the concentration increased, showing the largest differences for CO_2 concentrations above 50 vol. %.

For any AC, at low CO_2 concentrations, the most important pores for adsorption are the narrowest pores available, pores narrower than 0.6 nm are the most relevant when working at 15 % of CO_2 [14]. Samples MSP-20X and XiPPO_3 have a similar $V_{micro\ DR}$ (CO_2) and showed similar CO_2 uptakes at low concentrations. XPPO_1, at CO_2 concentrations higher than 15 vol. %, became the best sample due not only first to the highest $V_{micro\ DR}$, but also to its lowest $L_{0,\ NLDFT,}$ 0.72 nm). However, at CO_2 concentrations lower than 15 vol. %, XPPO_1 had the lowest capture capacity and the lowest pore volume between 0.7 and 50 nm. Consequently, when the CO_2 concentration increased, the contribution of pores less than or equal to 0.7 nm became important,

which means that all samples with a higher $V_{L<0.7}$ would show a higher CO_2 capture capacity, as indicated previously and as reported elsewhere [14, 39, 40].

For common CO_2 concentrations in combustion processes, both XPPO_1 and CWPO_1 had a similar behavior with respect to CO_2 capture.

3.5 CO_2 adsorption-desorption evaluation

For any CO_2 capture process, the ultimate practical objective is to determine the feasibility of the method over a large number of adsorption-desorption cycles. In the case of ACs for which CO_2 is physically adsorbed on the material, the increase of the temperature favors the desorption of CO_2 from the surface of the adsorbent and can also affect the stability of the carbon materials. The thermal stability of the best ACs considered in this study is illustrated in Figure S6.

There is first a drop of sample weight associated to the presence of moisture in the AC, followed by a progressive but slight decrease in weight between 8 and 10 % for CWPO_1 and XPPO_1, respectively, until stabilization. Therefore, the regeneration temperature used might have a negative effect on the CO_2 working capacity after the desorption step, as the structure and stability of the samples could be affected.

Figure 8 shows the variation of the weight according to the adsorption-desorption profiles for the sample XPPO_1 using an adsorption temperature of 25ºC and desorption temperatures of 125, 150, 175 or 200°C. It was observed that after the first cycle, the initial weight of the AC before CO_2 adsorption at each cycle was smaller as the desorption temperature increased. However, the CO_2 working capacity (2.47 mmol CO_2/g AC) was the same in all cycles, regardless of the desorption temperature. The same behavior was observed for all other ACs.

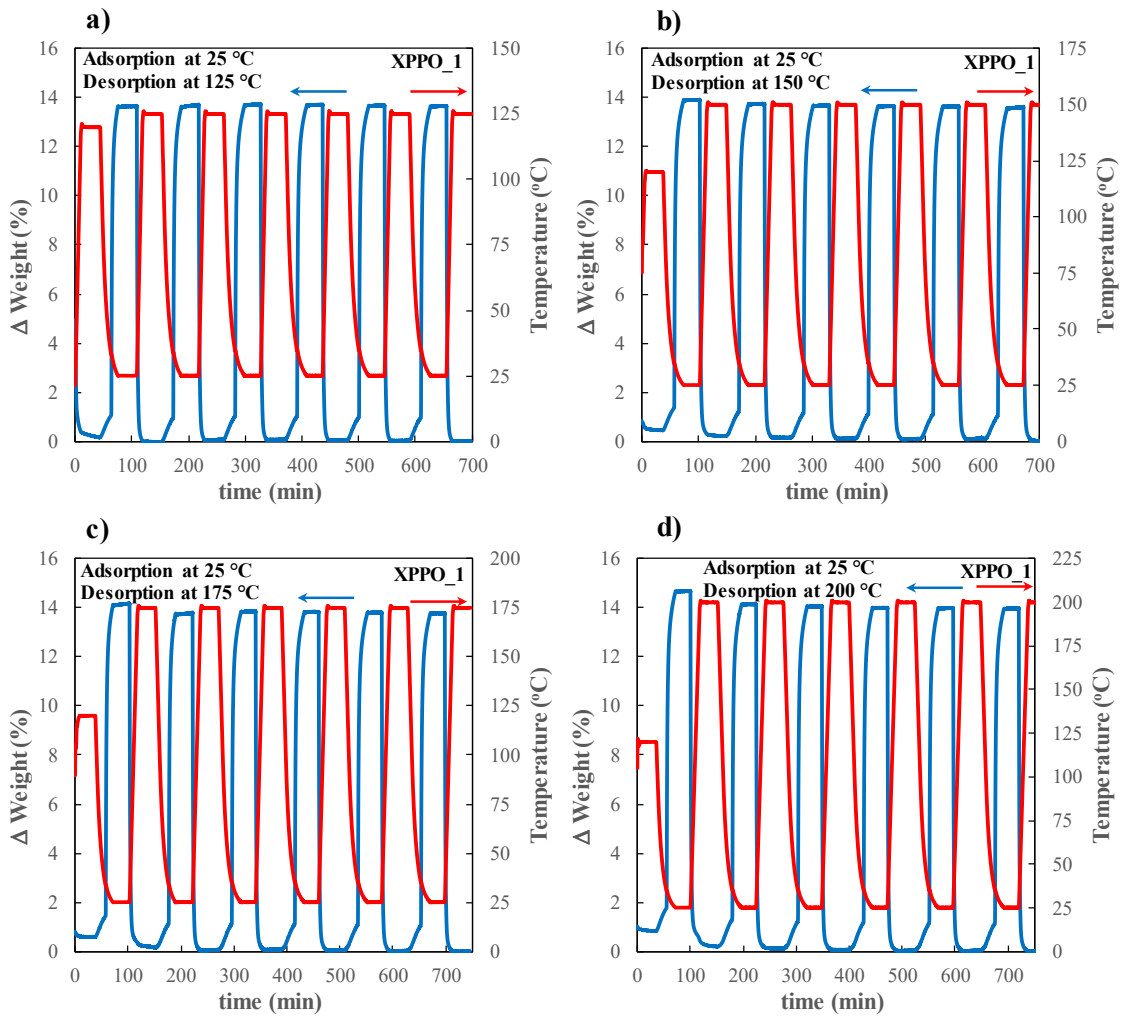

Figure 8. Adsorption-desorption cycles of the activated carbon XPPO_1, with adsorption at 25ºC and 90% CO_2 concentration and desorption at: a) 125ºC, b) 150ºC, c) 175ºC, and d) 200ºC.

Table 3 shows the CO_2 working capacity of the most efficient samples through 6 adsorption-desorption cycles at 200°C as a regeneration temperature chosen to evaluate the behavior of the materials at the highest temperature considered and their degradation during cycles. In all cases, the CO_2 working capacity remained constant, corroborating the stability of the samples upon cycling, even using a high temperature for the regeneration step.

Table 3. CO_2 working capture capacity of the most efficient samples at adsorption and desorption temperatures of 25ºC and 200ºC, respectively.

Number of cycle	MSP-20X mmol CO_2 / g AC	XiPPO_3 mmol CO_2 / g AC	XPPO_1 mmol CO_2 / g AC	CWPO_1 mmol CO_2 / g AC
1	2.68	2.51	2.86	2.73
2	2.68	2.48	2.88	2.66
3	2.68	2.46	2.88	2.65
4	2.61	2.46	2.88	2.68
5	2.68	2.48	2.88	2.69
6	2.66	2.42	2.89	2.72
Average	2.66 ± 0.02	2.47 ± 0.02	2.88 ± 0.003	2.69 ± 0.02

4. Conclusion

This work presents the development of different activated carbon xerogels and cryogels, all derived from a low-value industrial product, phenolic oil, for the capture of CO_2 under different conditions of adsorption temperature, CO_2 concentration, and regeneration temperature. Some of these samples showed higher CO_2 capture capacities than commercial activated carbons, with very good repeatability. The carbon xerogel produced with a basic catalyst and activated with a carbon/KOH ratio equal to 1:1 had the best CO_2 uptake (2.86 mmol/g AC). The second most efficient sample was the carbon cryogel activated under the same conditions. The obtained values in this study are indeed comparable to previously reported values for ACs without any modification/functionalization. Furthermore, the role of the textural properties of these new ACs on the CO_2 capture under different postcombustion conditions has been elucidated. Initially, it has been observed that two different samples with different surface areas and microporous fractions could present the same CO_2 capture capacity. Nevertheless, the influence

of the presence of micropores and, more importantly, narrow pores in the structure of the samples has been demonstrated as the main CO_2 capture factor at 25 °C, with a clear trend as the partial pressure of CO_2 increased. Therefore, if the microporous fraction was reduced during activation, the surface area should be high enough to maintain a constant CO_2 capture capacity. It was observed that two samples with different textural characteristics have similar CO_2 capture capacities.

However, as the temperature increased, it was determined that the presence of narrow pores had a lesser influence on CO_2 adsorption, and a higher surface area, total pore volume and absolute micropore volume become more important. This was justified by a polarized physisorption phenomenon taking place on the surface defects of the carbon surface. Moreover, it has been determined that as the partial pressure of CO_2 increases, getting values higher than 25 vol. %, the narrow and micropores get more relevance.

The stability of the best samples of each family selected in this work was evaluated up to a temperature of 220°C. It was determined that, as the temperature increased, there was a slight variation in the weight of the AC. However, it was also determined that the desorption temperature has no effect on the CO_2 capture capacity during cycles.

Finally, six adsorption-desorption cycles were carried out for each of the best samples at a regeneration temperature of 200°C. The repeatability and feasibility of samples for CO_2 capture was demonstrated in all cases, and the materials with the highest capacity at 25°C were the ones showing the best behavior upon cycling. These results highlighted the possibility of using activated carbon gels produced using phenolic oil as a relevant precursor for CO_2 capture.

ASSOCIATED CONTENT

Supporting Information

Reproducibility of CO_2 capture capacity values at 25ºC and 1 bar under a 90% CO_2 atmosphere, coefficients of multiple linear regressions for CO_2 adsorption at 25°C for four different pore classes, simple linear regression between adsorbed amounts of CO_2 at 25°C and pore volumes: a) VL<0.5, or b) V0.5<L<0.7, Steele, adsorption potential and effective pore size calculations, Steele adsorption potential for the CO_2 – graphite system (slit pores model), minimum of Steele's potential as a function of the distance between the median planes of the graphitic pore walls, adsorbed amount of CO_2 per unit of BET surface area as a function of the average micropore size calculated by application of the Dubinin-Radushkevich method ($L_{0,DR}$), ultramicropore fraction, supermicropore fraction and mesopore fraction, as a function of the average micropore size according to the NLDFT method, enthalpy of adsorption calculation for adsorbed CO_2 monolayer, Van't Hoff plot for CO_2 adsorption at a pressure of 10^5 Pa, and thermal stability of ACs from room temperature to 220ºC: a) MSP-20X, b) XiPPO_3, c) XPPO_1, and d) CWPO_1. The following files are available free of charge via the Internet at http://pubs.acs.org.

AUTHOR INFORMATION

Corresponding Author

*Susana Garcia. E-mail address: s.garcia@hw.ac.uk.

*Vanessa Fierro. E-mail address: vanessa.fierro@univ-lorraine.fr.

Present Addresses

† Research Centre for Carbon Solutions (RCCS), School of Engineering and Physical Sciences, Heriot-Watt University, Edinburgh EH14 4AS, United Kingdom

‡ Université de Lorraine, CNRS, IJL, F-88000 Epinal, France

ACKNOWLEDGMENT

This work is supported by the European Commission under the "Research Fund for Coal and Steel (RFCS)" Programme (Project No 709741).

REFERENCES

(1) "Recently Monthly Average Mauna Loa CO_2", NOAA, [Online]. Available: https://www.esrl.noaa.gov/gmd/ccgg/trends/.

(2) IPCC, "Global Warming of 1.5°C. Summary for Policymakers.", Intergovernamental Panel on Climate Change, Switzerland, **2018**.

(3) Wang, Q.; Luo, J.; Zhong, Z.; Borgna, A.; CO_2 Capture by Solid Adsorbents and their Applications: Current Status and Trends. *Energy Environ. Sci.* **2011**, 4, 42-55.

(4) Cuellar-Franca, R.; Azapagic, A. Carbon Capture, Storage and Utilisation Technologies: a Critical Analysis and Comparison of their Life Cycle Environmental Impacts. *J. CO_2 Util*. **2015**, 9, 82-102.

(5) Rashidi, N.; Yusup, S. An Overview of Activated Carbons Utilization for the Post-Combustion Carbon Dioxide Capture. *J. CO_2 Util*. **2016**, 13, 1-16.

(6) Plaza, M.; Garcia, S.; Rubiera, F.; Pis, J.; Pevida, C. Post-combustion CO_2 Capture with a Commercial Activated Carbon: Comparison of Different Regeneration Strategies. *Chem. Eng. J.* **2010**, 163, 41-47.

(7) Yu, C. H.; Huang, C. H.; Tan, C. S. A Review of CO_2 Capture by Absorption and Adsorption. *Aerosol and Air Quality Res.* **2012**, 12, 745-769.

(8) Lee, S. Y.; Park, S. J. Determination of the Optimal Pore Size for Improves CO_2 Adsorption in Activated Carbon Fibers. *J. Colloid Interface Sci.* **2013**, 389, 230-235.

(9) Drage, T.;Kozynchenko, O.; Pevida, C.; Plaza, M.; Rubiera, F.; Pis, J.; Snape, C.; Tennison, S. Developing Activated Carbon Adsorbents for Pre-Combustion CO_2 Capture. *Energy Procedia.* **2009**, 1, 599-605.

(10) Marsh, H.; Rodriguez-Reinoso, F. Activated Carbon, *Elsevier Sci.* **2006.**

(11) Maroto-Valer, M.; Lu, Z.; Zhang, Y.; Tang, Z. Sorbents for CO_2 Capture from High Carbon Fly Ashes. *Waste Management*. **2008**, 28, 2320-2328.

(12) Jimenez, V.; Sanchez, P.; Valverde, J.; Romero, A. Effect of the Nature the Carbon Precursor on the Physo-Chemical Characteristics of the Resulting Activated Carbon Materials. *Mater. Chem. Phys.* **2010**, 124, 223-233.

(13) Zhao, W.; Fierro, V.; Zlotea, C.; Aylon, E.; Izquierdo, M.; Latroche, M.; Celzard, A. Optimzation of Activated Carbons for Hydrogen Storage. *Int. J. Hydrogen Energy*. **2011**, 18, 11746-11751.

(14) Serafin, J.; Narkiewicz, U.; Morawski, A.; Wróbel, R.; Michalkiewicz, B. Highly Microporous Activated Carbons from Biomass for CO_2 Capture and Effective Micropores at Different Conditions. *J. CO_2 Util.* **2017**, 18, 73-79.

(15) Yaumi, A.; Abu Bakar, M.; Hameed, B. Recent Advances in Functionalized Composite Solid Materials for Carbon Dioxide Capture. *Energy.* **2017**, 124, 461-480.

(16) Nowrouzi, M.; Younesi, H.; Bahramifar, N. Superior CO_2 Capture Performance on Biomass-derived Carbon/Metal Oxides Nanocomposites from Persian Ironwood by H_3PO_4 Activation. *Fuel.* **2018**, 223, 99-114.

(17) Fadhil, A.; Ahmed, A.; Salih, H. Production of Liquid Fuels and Activated Carbons from Fish Wast. *Fuel.* **2017**, 187, 435-445.

(18) Jeder, A.; Sanchez-Sanchez, A.; Gadonneix, P.; Masson, E.; Ouederni, A.; Celzard, A.; Fierro, V. The Severity Factor as Useful Tool for Producing Hydrochars and Derived Carbon Materials. *Environ. Sci. Pollut. Res. Int.* **2018**, 25(2) 1497-1507.

(19) Taher, S.; Sanchez-Sanchez, A.; Gadonneix, P.; Jagiello, J.; Seffen, M.; Sammouda, H.; Celzard, A.; Fierro, V. Tetracycline Removal with Activated Carbons Produced by

Hydrothermal Carbonisation of Agave Americana Fibres and Mimosa Tannin. *Industrial Crops and products.* **2018**, 115, 146-157.

(20) Schaefer, S.; Muñiz, G.; Izquierdo, M.; Mathieu, S.; Ballinas-Casarrubias, M.; Gonzalez-Sanchez, G.; Celzard, A.; Fierro,. V. Rice Straw-based Activated Carbons Doped with SiC for Enhanced Hydrogen Adsorption. *Int. J. Hydrogen Energy*. **2017**, 42(16), 11534-11540.

(21) Wang, J.; Heerwig, A.; Lohe, M.; Oschatz, M.; Borchardt, L.; Kaskel, S. Fungi-based Porous Carbons for CO_2 Adsorption and Separation. *J. Mater. Chem.* **2012**, 22, 13911-13913.

(22) Sevilla, M.; Fuertes, A. Sustainable Porous Carbons with a Superior Performance for CO_2 Capture. *Energy Environ. Sci.* **2011**, 4, 1765-1771.

(23) Marco-Lozar, J.; Kunowsky, M.; Suarez-Garcia, F.; Lianres-Solano, A. Sorbent Design for CO_2 Capture under Different Flue Gas Conditions. *Carbon.* **2014**, 72, 125-134.

(24) Reynolds, G.; Fung, A.; Wang, Z.; Dresselhaus, M.; Pekala, R. The Effects of External Conditions on the Internal Structure of Carbon Aerogels. *J. Non-Cryst. Solids*. **1995**, 188, 27-33.

(25) Pekala, R.; Alviso, C.; Lu, X.; Fricke, J. New Organic Aerogels Based upon a Phenolic-Furfal Reaction. *J. Non-Cryst. Solids.* **1995**, 188, 34-40.

(26) Robertson, C.; Mokaya, R. Microporous Activated Carbon Aerogels via a simple Subcritical Drying Route for CO_2 Capture and Hydrogen Storage. *Microporous Mater.* **2013**, 179, 151-156.

(27) Lee, K.; Sircar, S. Removal and Recovery of Compressed CO_2 from Flue Gas by a Novel Thermal Swing Chemisorption Process. *AIChE. J.* **2008**, 54, 2293-2302.

(28) Choi, S.; Drese, J.; Jones, C. Adsorbent Materials for Carbon Dioxide Capture from Large Anthropogenic Point Sources. *Chem. SusChem*. **2009**, 2, 796-854.

(29) Brunauer, S.; Emmet, P.; Teller, E. Adsorption in Multimolecular Layers. *J. Am. Chem. Soc.* **1938**, 60, 2, 309-319.

(30) Thommes, M.; Kaneto, K.; Neimark, A.; Olivier, J.; Rodriguez-Reinoso, F.; Rouquerol, J.; Sing, K. Physisorption of Gases, with Special Reference to the Evaluation of Surface Area and Pore Size Distribution (IUPAC Technical Report). *Pure and Appl. Chem.* **2015**, 87, 1051-1069.

(31) Dubinin, N. Fundamentals of the Theory of Adsorption in Micropores of Carbon Adsorbents: Characteristics of their Adsorption Properties and Microporous Structures. *Carbon*. **1989**, 27(3), 457-467.

(32) Chen, S.; Yang, R. Theoretical Basis for the Potential-theory Adsorption Isotherms-The Dubinin-Radushkevich and Dubinin-Astakhov Equations. *Langmuir*. **1994**, 10(11), 4244-4249.

(33) Hutson, N.; Yang, R. Theoretical Basis for the Dubinin-Radushkevitch (D-R) Adsorption Isotherm Equation. *Adsorption-J. of the Int. Adsorption Soc.* **1997**, 3(3), 189-195.

(34) Jagiello, J.; Ania, C.; Parra, J.; Cook, C. Dual Gas Analysis of Microporous Carbons using 2D-NLDFT Heterogeneous Surface Model and Combined Adsorption Data of N_2 and CO_2. *Carbon*. **2015**, 91, 330-337.

(35) Stoeckli, F. *Porosity in carbon. Characterization and applications.* Eds. Patrick. Arnold, J. **1995**, London

(36) Centeno, T.; Stoecki, F. The Assessment of Surface Areas in Porous Carbons by two Model-independent Techniques, the DR equation and DFT. *Carbon*. **2010**, 48(9), 2478-2486.

(37) Fierro, V.; Szczurek, A.; Zlotea, C.; Mareche, J.; Izquierdo, M.; Albiniak, A.; Latroche, M.; Furdin, G.; Celzard, A. Experimental Evidence of an Upper Limit for Hydrogen Storage at 77 K on Activated Carbons. *Carbon.* **2010**, 48, 1902-1911.

(38) Jalilov, A.S.; Ruan, G.; Hwang, C.-C.; Schipper, D.E.; Tour, J.J.; Li, Y.; Fei, H.; Samuel, E.; Tour, J.M. Asphalt-Derived High Surface Area Activated Porous Carbons for Carbon Dioxide Capture. *ACS Appl. Mater. & Interfaces*. **2015**, 7(2), 1376-1382.

(39) Martin, C.; Plaza, M.; Pis, J.; Rubiera, F.; Pevida, C.; Centeno, T. On the Limits of CO_2 Capture Capacity of Carbons. *Separation and purification Techn.* **2010**, 74, 225-229.

(40) Casco, M.; Martinez-Escandell, M.; Silvestre-Albero, J.; Rodriguez-Reinoso, F. Effect of the Porous Structure in Carbon Materials for CO_2 Capture at Atmospheric and High-Pressure. *Carbon*. **2014**, 67, 230-235.

(41) Zhao, W.; Fierro, V.; Zlotea, C.; Aylon, E.; Izquierdo, M.; Latroche, M.; Celzard, A. Activated Carbons with Appropriate Micropore Size Distribution for Hydrogen Adsorption. *Int. J. Hydrogen Energy.* **2011**, 36(9), 5431-5434.

(42) Schaefer S.; Fierro, V.; Izquierdo, M.; Celzard, A. Assessment of Hydrogen Storage in Activated Carbons produced from Hydrothermally Treated Organic Materials. *Int. J. Hydrogen Energy.* **2016**, 41(28), 12146-12156.

(43) Steele, W. Physical interaction of gases with crystalline solids. 1. Gas solid Energies and Properties of Isolated Adsorbed Atoms. *Surface Sci.* **1973**, 36(1), 317-352.

(44) Kurniawan, Y.; Bhatia, S.; Rudolp, V. Simulation of Binary Mixture Adsorption of Methane and CO_2 at Supercritical Conditions in Carbons. *Aiche J.* **2006**, 52(3), 957-967.

(45) Ravikovitch, P.; Vishnyakov, A.; Russo, R.; Neimark, A. Unified Approach to Pore Size Characterization of Microporous Carbonaceous Materials from N_2, Ar and CO_2 Adsorption Isotherms. *Langmuir.* **2000**, 16(5), 2311-2320.

(46) Chen, L.; Watanabe, T.; Kanoh, H.; Hata, K.; Ohba, T. Cooperative CO_2 Adsorption Promotes high CO_2 Adsorption Density over wide Optimal Nanopore Range. *Adsorption Sci. & Techn.* **2018**, 36 (1-2), 625-639.

(47) Kaneko, K.; Cracknell, R.; Nicholson, D. Nitrogen Adsorption in Slit Pores at Ambient Temperatures-comparison of Simulation and Experiment. *Langmuir*. **1994**, 10(12), 4606-4609.

(48) Kaneko, K. Specific Intermolecular Structures of Gases Confined in Carbon Nanospace. *Carbon.* **2000**, 38(2), 287-303.

(49) Sevilla, M.; Mokaya, R. Energy Storage Applications of Activated Carbons: Supercapacitors and Hydrogen Storage. *Energy & Environ. Sci.* **2014**, 7(4), 1250-1280.

(50) Schaefer, S.; Muñiz, G.; Izquierdo, M.; Mathieu, S.; Ballinas-Casarrubias, M.; Gonzalez-Snachez, S.; Celzard, A.; Fierro, V. Rice Straw-based Activated Carbons Doped with SiC for Enhanced Hydrogen Adsorption. *Int. J. Hydrogen Energy*. **2017**, 42(16), 11534-11540.

(51) Sevilla, M.; Parra, J.B.; Fuertes, B. Assessment of the Role of Micropore Size and N-Doping in CO_2 Capture by Porous Carbons. *ACS Appl. Mater. & Interfaces*. **2013**, 5, 6360-6368.

(52) Arenillas, A.; Smith, K.; Drage, T.; Snape, C. CO_2 Capture Using some Fly Ash-Derived Carbon Materials. *Fuel*. **2005**, 84, 2204-2210.

(53) Trinh, T.; van Erp, T.; Bedeaux, D.; Kjelstrup, S.; Grande, C. A Procedure to find Thermodynamic Equilibrium Constants for CO_2 and CH_4 Adsorption on Activated Carbon. *Physical Chem. Chem. Physics*. **2015**, 17(12), 8223-8230.

(54) Himeno, S.; Komatsu, T.; Fujita, S. High-pressure Adsorption Equilibria of Methane and Carbon Dioxide on Several Activated Carbons. *J. Chem. and Eng. Data.* **2005**, 50(2), 369-376.

(55) Radovic, L. The Mechanism of CO_2 Chemisorption on Zigzag Carbon Activate Sites: A Computational Chemistry Study. *Carbon.* **2005**, 43(5), 907-915.

(56) Liu, Y.; Wilcox, J. Effects of Surface Heterogeneity on Adsorption of CO_2 in Microporous Carbons. *Environ. Sci. & Techn.* **2012**, 46(3), 1940-1947.

FOR TABLE OF CONTENTS ONLY (TOC/ ABSTRACT GRAPHIC)